Spill ripple mitigation by bunched beam extraction with high frequency synchrotron motion

S. Sorge,* P. Forck, and R. Singh

GSI Helmholtzzentrum f. Schwerionenforschung GmbH, Planckstraße 1, 64291 Darmstadt, Germany

(Received 15 March 2022; accepted 3 January 2023; published 19 January 2023)

Slow extraction of bunched beams is widely used for mitigating the formation of temporal microstructures on the extracted beam due to ripples of the accelerator magnets power supplies. That helps in experiments with slow detectors or measurements with low event rates. Additionally, in ion cancer therapy machines, this technique is widely used for avoiding long gaps in the spill measured in ionization chambers which in turn would trigger interlocks. It is also well known that extraction of a bunched beam creates spill structures on time scales defined by the rf frequency which limits its usability for faster detectors. In this report, we show that further macroscopic spill structures of duration up to some hundred milliseconds can be created during bunched beam extraction for a sufficiently large synchrotron tune. The aim of this work is to study the influence of the synchrotron tune and its interplay with slow extraction settings on the slow extraction quality. Further dependencies on transverse emittance and longitudinal bunch area of the circulating beam are discussed.

DOI: 10.1103/PhysRevAccelBeams.26.014402

I. INTRODUCTION

Slow extraction from synchrotrons and storage rings is widely used for delivering hadron beams to many fixed target experiments as well as for the irradiation of tumors in hadron cancer therapy. A third integer lattice resonance is used for most slow extractions. This resonance is excited by sextupole magnets in the ring and forms a triangular area in the transverse phase space plane used for the extraction separating the unstable betatron motion outside and the stable betatron motion inside. That triangular area is referred to as a stable phase space area. The extraction is executed by subsequent feeding the resonance which means that the particles are successively pushed out of that stable phase space area. Thereby, their betatron motion becomes unstable, they leave the beam, and become extracted by reaching the extraction septum. The extracted beam is also referred to as a spill. Typical extraction time intervals reach from some hundred milliseconds up to hours. Several resonance feeding techniques are presently in operation such as tune sweep [1], betatron core driven [1,2], and rf knockout extraction [3]. The first two mechanisms are based on the reduction of the size of the stable phase space area, whereas in the last method, the betatron amplitudes of the particles are slowly increased beyond the edge of the stable phase space area. The choice of the resonance feeding mechanism depends on the parameters of the beam required by the users such as beam energy and intensity, spill duration, or safety requirements like the ability to suddenly interrupt the extraction if the spill is utilized for the irradiation of patients in medical facilities. A frequent user requirement for the spill is a low level of undesired temporal structures. Ripples and noise on the current supplied to the accelerator quadrupole magnets could be identified as major sources of fluctuations in the machine tune. They translate in a ripple on the size of the stable phase space area and, hence, in temporal structures on the particle flow out of the stable phase space area. These spill microstructures have a characteristic time from ~ 10 ms down to ~ 10 μs which is too short to be efficiently mitigated by a feedback system [4,5] and significantly longer than the revolution time.

The particles need a certain time T_{tr} after leaving the stable phase space area for the transit to the extraction septum. These transit times are not uniform due to a spread of the particle momenta and the resulting chromatic tune changes. The width of the resulting transit time distribution defines a transit time spread ΔT_{tr}. Thereby, temporal structures formed by particles that leave the stable phase space area at the same instant are smeared out [6]. That mechanism can be utilized for the reduction of spill microstructures while applying an extraction technique that does not rely on longitudinal dynamics, for example, slow extraction of unbunched beams by tune sweep [7].

Other major approaches for mitigating spill microstructures work with help of longitudinal dynamics. These

*S.Sorge@gsi.de

techniques are based on the change of the momenta and, thus, the chromatic tune deviations of particles toward the resonance tune by rf fields. The resulting transition of particles across the edge of the stable phase space area is much faster than that caused by resonance feeding [6]. Thereby, the duration of stay of particles near the separatrix is shorter and the level of structures imprinted on the particle flux out of the stable phase space area is reduced. Spill microstructure reduction can be achieved due to quickly changing particle momenta by applying rf fields of defined harmonic number resulting in synchrotron motion during slow extraction of bunched beams [8,9] or passing between empty rf buckets in rf phase displacement and empty bucket channeling techniques [1,2,10]. Longitudinal diffusion is driven by rf noise with a band limited power spectrum during stochastic extraction [11].

It is worth mentioning that the creation of spill structures shorter than a revolution time by bunched beam slow extraction or particles passing between empty buckets was earlier proposed and studied for the purpose to suppress the particle background in user experiments, see, e.g., [12–14]. Now, such techniques are on the way to the application [15–17].

Contrary to those studies, the sole aim of the present work is to study the formation and mitigation of spill structures during the slow extraction of bunched ion beams from the present heavy ion synchrotron SIS18 of the GSI facility within a simulation study. The work is restricted to slow extraction by tune sweep performed with two fast ramped quadrupoles because that is the standard slow extraction technique of SIS18. The focus is on the investigation of the influence of synchrotron motion significantly faster than usually applied in the present operation at SIS18 and various therapy machines. This topic is motivated by the plan to install a high frequency rf cavity in order to provide rf fields with a harmonic number increased by an order of magnitude [18] which is required by an experiment collaboration with high event rates [19]. The goal is to take advantage of the spill microstructure reduction provided by bunched beam extraction while avoiding spill structures at typical present rf frequencies [20,21]. Hence, the aim of our study is to demonstrate the applicability of the high frequency rf cavity in SIS18 and to point out some limitations to the operation.

II. CONDITIONS FOR SLOW EXTRACTION FROM SIS18 ASSUMED IN THE STUDY

Slow extraction from SIS18 is based on the formation of a triangular stable area in the horizontal phase space plane by exciting a one-dimensional third integer resonance with sextupoles. This process can be described by the Kobayashi theory [22]. The size of the stable phase space area is given by its corners which are unstable fixed points (UFPs) of betatron motion. Written in normalized coordinates of the phase space vector $\vec{X} = (X, X')$ with

$$X \equiv \frac{x}{\sqrt{\beta_x}} \quad \text{and} \quad X' \equiv \sqrt{\beta_x}x' + \frac{\alpha_x}{\sqrt{\beta_x}}x, \tag{1}$$

see, e.g., [1,23,24], the UFPs have all the same absolute value

$$|\vec{X}_{\mathrm{UFP}}| = 8\pi\left|\frac{Q_\mathrm{r} - Q_\mathrm{p}}{S_\mathrm{v}}\right|, \tag{2}$$

where Q_r and Q_p are resonance tune and on-axis tune of the particles. The latter can be modified by chromaticity ξ and relative momentum deviation δ of the particles to

$$Q_\mathrm{p} \equiv Q_\mathrm{m} + \xi\delta. \tag{3}$$

S_v in Eq. (2) is the strength of a virtual sextupole and is given by

$$S_\mathrm{v}\mathrm{e}^{3\mathrm{i}\psi_\mathrm{v}} = \sum_n S_n \mathrm{e}^{3\mathrm{i}\psi_n} \tag{4}$$

with the normalized strength of the nth sextupole

$$S_n = \frac{1}{2}\beta_{x,n}^{3/2}(k_2 L)_n \tag{5}$$

and the betatron phase advance ψ_n between the location of the nth sextupole and the considered location which is usually the entrance of the electrostatic septum. The ψ_n has to be determined for the third integer tune of the resonance Q_r. The resulting size of the stable phase space area is

$$A_\mathrm{stable} = 3\frac{1}{2}|\vec{X}_{\mathrm{UFP}}|^2 \sin 120° = \frac{\sqrt{27}}{4}|\vec{X}_{\mathrm{UFP}}|^2. \tag{6}$$

The corresponding emittance is

$$\epsilon_\mathrm{stable} = \frac{A_\mathrm{stable}}{\pi}. \tag{7}$$

The dependence of A_stable on the tune can be used for extracting the beam by moving the machine tune Q_m slowly across the resonance tune due to changing the focusing strengths of quadrupoles. Thereby, A_stable shrinks and the particles become successively unstable according to their transverse emittance and momentum dependent tune such that they leave the synchrotron. This technique referred to as quadrupole driven extraction is the present standard technique for slow extraction from SIS18. Hence, this study is focused on the usage of this method. Typical beam and lattice parameters for the extraction from SIS18 used in our study are presented in Table I.

A comprehensive series of machine experiments was performed with beams of Ar^{18+} ions at the beam energy $E = 500$ MeV/u. Typical extraction rates were between 10^5 and 10^6 ions/s. The choice of these extraction rates is

TABLE I. Typical beam and lattice parameters used in experiments and simulations.

Circumference of synchrotron	$C = 216.72$ m
Chromaticities (h, v) according to Eq. (8)	$\xi_x = -5.7$, $\xi_y = -5.0$
Momentum compaction factor	$\alpha_0 = 0.033$
Ion	Ar^{18+}
Beam energy	$E = 500$ MeV/u
Lorentz factors	$\gamma_0 = 1.54$, $\beta_0 = 0.76$
Maximum emittances (h, v)	$\epsilon_{x,\max} = 15.6$ mm mrad, $\epsilon_{y,\max} = 5.2$ mm mrad
Maximum relative momentum deviation	$\delta_m = 5.0 \times 10^{-4}$
Extraction duration	
Experiments	5 s
Simulations	0.5 s
Extraction rate	
Experiments	$\sim 10^6$/s
Simulations	2.0×10^5/s

motivated by several reasons: (i) It allows for longer usage of the plastic scintillation counter for measuring the spill. (ii) It is well below its threshold of counting rates even in presence of pileups and thus allowing almost noise-free measurements. (iii) It provides the opportunity to perform particle tracking simulations with particle numbers similar to those of the measurements in a reasonable amount of time. We have simulated these measurement conditions in the present study for closer comparison to the experiments.

III. SPILL SIMULATIONS AND CHARACTERIZATION OF SPILL MICROSTRUCTURES

Spill structures can be investigated by simulating the process of slow extraction with particle tracking. We use the thin lens tracking module of the MAD-X code for the simulations. A key ingredient is the usage of the update option of MAD-X in order to change lattice parameters during a tracking simulation. It is applied at the beginning of the simulation to turn on the rf voltage as well as the strength of the sextupoles within a "preparation phase" of 50,000 revolutions duration along a linear ramp. In the subsequent extraction, the strength of two quadrupoles is linearly in time changed in order to move the horizontal tune from the initial to the final value with a constant tune change rate. Also, the quadrupole ripple signal is introduced by applying the update option. The quadrupole ripple signal consists of a sinusoidal contribution with a frequency of 600 Hz and a noise signal with a bandwidth limited to 10 kHz. The amplitudes of the sinusoidal contribution as well as the rms signal strength of the noise signal are 0.67×10^{-5} of the strength of the main quadrupoles. The choice of the frequency of 600 Hz is motivated by the design of the power supplies of the quadrupoles which allow the transmission of 600 Hz as the lowest multiple of the power grid frequency of 50 Hz. These values were comparable to ripple amplitude estimates in previous measurements [25]. The quadrupole ripple signal is introduced by a thin quadrupole element placed in the center of each quadrupole.

10^5 particles are tracked in each simulation for 5×10^5 revolutions after finishing the bunching process.

According to the initial conditions with $V_{\rm rf} = 0$, the spatial longitudinal particle coordinates are distributed uniformly in a range of the length $l = C/h$, where C is the ring circumference and h is the harmonic number of the rf frequency. The relative momentum deviations are set according to a Gaussian distribution truncated at $\pm 2\sigma$ with a typical maximum momentum deviation $\delta_m = 5 \times 10^{-5}$. The resulting maximum chromatic tune deviations $\Delta Q_{x,m}$ and $\Delta Q_{y,m}$ are determined by

$$\Delta Q_z = \xi_z \delta, \tag{8}$$

where $z = x, y$. In the simulations for the present study, always the natural chromaticities $\xi_x = \xi_{x,\rm nat} = -5.7$ and $\xi_y = \xi_{y,\rm nat} = -5.0$ are used which leads to $\Delta Q_{x,m} = 0.0029$ and $\Delta Q_{y,m} = 0.0025$. Both the maximum momentum deviation as well as the maximum tune deviations are increased by the bunch formation.

The initial transverse coordinates are set according to Gaussian distributions truncated at $\pm 2\sigma$ as well. The σ values of the corresponding Gaussian functions are defined by the rms beam emittances $\epsilon_{x,\rm rms} = 3.9$ mm mrad and $\epsilon_{y,\rm rms} = 1.3$ mm mrad. The resulting maximum beam emittances are $\epsilon_{x,\max} = 15.6$ mm mrad and $\epsilon_{y,\max} = 5.2$ mm mrad, respectively. They arise from the beam width given by the machine acceptance during injection and subsequent adiabatic shrinkage during acceleration. In some simulations, the maximum momentum deviation or the rms beam emittances are reduced in order to study their influence.

The spills are determined using the `trackloss` output of MAD-X. Only the revolution number is used for calculating the extraction time of each particle, whereas the modification due to the offset of a particle with respect to the synchronous particle is neglected. We apply this approximation because the time intervals for measuring the spills are much larger than a revolution time. The duration of these time intervals is given by the sampling rate of the spill measurement system, where $f_{\rm sample} = 100$ kHz in SIS18.

The quantity used in this study for characterizing the spill quality is the time dependent duty factor [25]

$$F(t) = \frac{\langle N \rangle^2(t)}{\langle N^2 \rangle(t)} = \frac{N_{\rm av}^2(t)}{N_{\rm av}^2(t) + \sigma_N^2(t)}. \tag{9}$$

$\langle x \rangle$ denotes the average of the variable x given in time intervals according to the measurement resolution $t_{\mathrm{meas}} = 1/f_{\mathrm{sample}}$ in time intervals t_{av}. The actual size of the measurement and averaging time intervals used for this study is $t_{\mathrm{meas}} = 10\ \mu\mathrm{s}$ and $t_{\mathrm{av}} = 10\ \mathrm{ms}$. A good spill quality is given by a low spill structure level and results in a large value of the time dependent duty factor.

The upper limit to $F(t)$ under realistic beam conditions and for $t_{\mathrm{av}} \gg t_{\mathrm{meas}}$ is reached in the Poisson limit $F_{\mathrm{P}}(t)$ which denotes a stochastic distribution of extracted particles in the measurement time intervals. For the probability to find N particles in a measurement time interval according to Poisson's distribution

$$f_{\mathrm{P}}(N) = \mathrm{e}^{-\lambda}\frac{\lambda^N}{N!}, \tag{10}$$

one finds $N_{\mathrm{av}}^2 + \sigma_N^2 = (N^2)_{\mathrm{av}} = N_{\mathrm{av}}(N_{\mathrm{av}} + 1)$ such that

$$F_{\mathrm{P}}(t) = \frac{N_{\mathrm{av}}(t)}{N_{\mathrm{av}}(t) + 1}. \tag{11}$$

It can be useful to reduce the time dependent duty factor to the averaged or weighted factor defined in [7] by

$$F_{\mathrm{av}} = \frac{\int \mathrm{d}t\, \dot{N}(t) F(t)}{\int \mathrm{d}t\, \dot{N}(t)} = \frac{\sum_k N_k F_k}{\sum_k N_k}. \tag{12}$$

$\dot{N}(t)$ is the time dependent particle extraction rate and represents the spill. By applying $N_k \equiv N_{\mathrm{av}}(t_k) = \langle \dot{N} \rangle (t_k) \cdot t_{\mathrm{av}}$ with $t_k = k \cdot t_{\mathrm{av}}$, the integrals can be replaced with the sums in the second row of Eq. (12).

IV. MITIGATION OF SPILL MICROSTRUCTURES WITH BUNCHING

Spill smoothing for bunched beam slow extraction is mainly based on the periodic change of the particles' tune due to synchrotron motion. The resulting transition from stable to unstable betatron motion is significantly faster than caused by the tune sweep. For typical synchrotron frequencies between 0.01% and 0.1% of the rf frequency, the particles are supposed to stay much shorter near the oscillating edge of the stable phase space area such that resulting structures imprinted on the spill are strongly reduced.

Following this reasoning, one would expect that an increase of the synchrotron tune Q_{s} would always result in an improvement of the spill quality or, at least, the improvement will saturate because the time the particles are near the separatrix has a lower limit. However, it is found in the particle tracking simulations, that the spill quality is improved only up to a certain optimum of Q_{s} and degraded when increasing Q_{s} further. That can be seen from the weighted duty factor according to Eq. (12) shown in Fig. 1 as a function of the synchrotron tune in small synchrotron amplitude approximation [26]

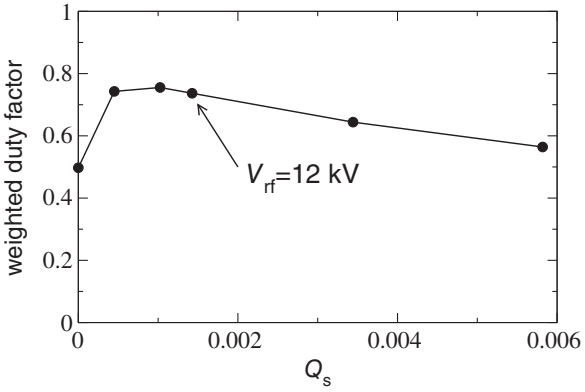

FIG. 1. Weighted duty factors according to Eq. (12) of spills obtained in simulations of the slow extraction of Ar^{18+} beams from SIS18 at the beam energy $E = 500\ \mathrm{MeV/u}$ as a function of the synchrotron tune according to the rf voltages $V_{\mathrm{rf}} = (0, 1.2, 6.2, 12, 70, 200)\ \mathrm{kV}$, where $V_{\mathrm{rf}} = 12\ \mathrm{kV}$ is the maximum which can be reached in SIS18. The rf voltage at the beginning of the simulations is switched off and slowly turned on during the first 50,000 turns. The initial maximum momentum deviation is $\delta_{\mathrm{m}} = 5 \times 10^{-4}$ and is increased during the bunching process. Hence, also longitudinal dynamics with low rf voltages with particles captured and others not captured in the rf bucket are well described.

$$Q_{\mathrm{s}} = \sqrt{\frac{hqV_{\mathrm{rf}}|\eta|\cos\phi_{\mathrm{s}}}{2\pi\beta_0^2 E_{\mathrm{tot}}}} \tag{13}$$

with the harmonic number of the rf frequency h, the amplitude of the rf voltage V_{rf}, the charge of the particles q, the phase slip factor η, the synchrotron phase of the synchronous particle ϕ_{s}, and the total energy of the particles E_{tot}. A qualitative explanation of this result is provided by the observation that particles are recaptured into the stable phase space area by the synchrotron motion after becoming unstable such that they cannot be extracted. The probability for particles to become recaptured is determined by their time of stay outside the stable phase space area Δt during a synchrotron period. The dependence of Δt on Q_{s} is qualitatively discussed in the following.

Let us consider a single particle which is at a certain instant t at that cusp of the synchrotron motion, where its tune including the chromatic correction is closest to the resonance tune. If in addition, this particle is assumed to be during t at the frontier between stable and unstable betatron motion represented by the larger triangle in the upper graph of Fig. 2, then the corresponding distance $X_{\mathrm{sep}}(t)$ of the separatrices from the beam center in normalized coordinates is represented by the upper straight black line in the

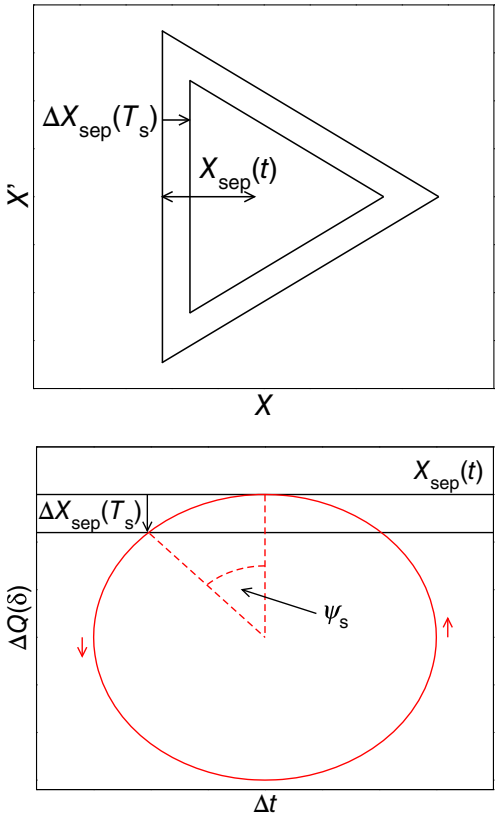

FIG. 2. Upper graph: Schematic plot of the stable phase space area at instant t and shrunk within a synchrotron period T_s by moving the machine tune $Q_{x,m}$ toward the resonance tune $Q_{x,r}$. Lower graph: Range of longitudinal coordinates of particles with certain horizontal emittance related to the distance of the separatrix from the beam center $X_{sep}(t)$ at instant t and shrunk within a synchrotron period T_s by $\Delta X_{sep}(T_s)$.

lower graph of Fig. 2. In such a case, the time of stay is determined by synchrotron phase $2\psi_s$ the particle passes during the stay by

$$\Delta t \propto T_s \psi_s. \tag{14}$$

This phase is governed by the reduction of the size of the stable phase area in a synchrotron period $\Delta X_{sep}(T_s)$ by means of the relation

$$\sin \psi_s \propto \Delta X_{sep}(T_s) \tag{15}$$

Assuming $\psi_s \ll 1$ and a constant tune ramp rate yields $\Delta X_{sep} \propto T_s$. The resulting time of the particles' first stay outside the stable phase space area

$$\Delta t \propto T_s^2 \propto \frac{1}{Q_s^2} \tag{16}$$

is shorter for faster synchrotron motion which translates in a higher probability for the particle to become recaptured.

The separatrix moves on in each further synchrotron period by $\Delta X_{sep}(T_s)$. If neglecting the increase of the betatron amplitude of the particle in each further stay, ψ_s after n synchrotron periods is given by

$$\sin \psi_s(n) \propto n \Delta X_{sep}(T_s). \tag{17}$$

which translates in the growth of the time of the particles' stay outside the stable area

$$\Delta t(n) \propto \frac{n}{Q_s^2}. \tag{18}$$

In addition, the distance of the particle from the separatrix while staying outside the stable phase space area grows in each synchrotron period which results in a shorter transit time. That is found for coasting beam conditions in simulations and agrees with the comprehensive sections with analytic transit time formulas found in [1,24]. A comparable derivation of transit times for particles under influence of longitudinal rf fields is not available and is well outside the scope of our paper.

Due to the increase in the time of stay and the decrease of the transit time in every synchrotron period, the particle will become extracted after some synchrotron periods. Both processes occur in smaller steps for a larger synchrotron tune. Consequently, the final extraction counted from the first crossing of the stable phase space boundary will take more synchrotron periods. In the meanwhile, the particle will stay under the influence of the separatrix oscillations. Hence, the recapture of particles counteracts the faster transition of the particles from stable to unstable betatron motion and explains the optimum in synchrotron tune in order to reduce spill microstructures.

The necessity for choosing a large synchrotron tune is introduced for the example of the high frequency cavity in the following section.

V. SPILL NANOSTRUCTURES

The improvement of the spill quality on microscopic time scales due to bunching occurs at the price of the creation of spill structures on time scales defined by the rf frequency

$$f_{rf} = f_{rev} h. \tag{19}$$

f_{rev} and h in this equation are revolution frequency and the harmonic number of the rf frequency. The rf frequency of the present SIS18 rf cavity reaches up to $f_{rf} = 6$ MHz [27]. According to a typical revolution time $t_{rev} \in [0.8, 1.0]$ μs during extraction, the rf harmonic number is usually $h = 4$ or $h = 5$ and the total duration of an rf bucket is $t_{bucket} \in [200, 250]$ ns. Hence, these structures are referred to as spill nanostructures.

The length of the bunches in the extracted beam is found to be shorter than that in the circulating beam [28]. The reason is that only particles are extracted which are near the cusp of synchrotron motion such that their chromatic tune reaches the phase space range of unstable betatron motion. This range corresponds to the area in the ellipse shown in the schematic plot in the lower graph of Fig. 2 which is between the black solid lines. It is shorter than the circulating bunch. In addition, most particles will start with their transit toward the extraction channel when they have passed the cusp of synchrotron motion because that point is in the greatest distance from the stable phase space range. For that reason, particles will reach the extraction channel in the shortest time when the transit starts there. Hence, most particles will arrive in an interval around the arrival time of the synchronous particle which is shorter and slightly delayed with respect to the arrival time of the synchronous particle. An example of profiles of circulating and extracted bunches obtained from simulation data is shown in Fig. 3. The length given by the full length at half maximum intensity of the circulating bunch under the chosen conditions is about $t_{b,\mathrm{circ}} = 84$ ns, whereas that of the extracted bunch integrated over the whole extraction process is $t_{b,\mathrm{ex}} = 40$ ns. The full bucket length is $t_{\mathrm{bucket}} = 190$ ns such that the duration of the void between two bunches is $t_{\mathrm{void,circ}} = 106$ ns for the circulating beam and even $t_{\mathrm{void,ex}} = 150$ ns for the extracted beam. In addition, one should note that the extracted bunch in Fig. 3 is obtained by accumulating the arrival times of the particles with respect to the synchronous particle of all extracted bunches. The resulting "accumulated" bunch is longer than a single extracted bunch. As a result, the intensity of the beam arriving at the target will have a stronger variability than suggested by that curve. That limits the maximum intensity and, hence, the event rate of some experiments

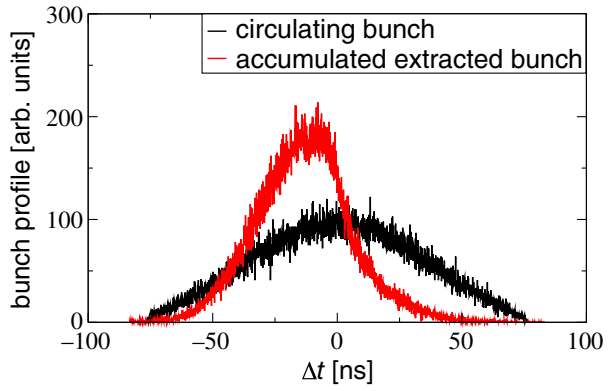

FIG. 3. Intensity profiles as a function of the time difference to the synchronous particle of a circulating bunch and the sum of all bunches extracted during the whole extraction process. In doing so, an accumulated extracted bunch profile is obtained which represents the same particle number as the profile of the circulating bunch. The profiles are obtained in a simulation for conditions used in Fig. 1 with $h = 5$ and $V_{\mathrm{rf}} = 6.2$ kV.

because the integration time of the detector is comparable to or shorter than the duration of a bunch. For example, the HADES detector [19] has an integration time of $t_{\mathrm{int}} = 140$ ns. For that reason, the number of particles detected in an integration time will be given by the maximum intensity which can lead to a pileup in case of a too large averaged intensity. On the other hand, no particles will be counted when a void is detected which means a waste of detection capacity [20,21]. A possible solution is to increase the rf frequency to a higher value that is matched to the detector rates. In this context, the installation of an rf cavity with a frequency $f_{\mathrm{rf}} = 80$ MHz is planned [18]. The choice of the cavity frequency was based on spare available GSI LINAC cavities. The duration of an rf bucket is $t_{\mathrm{bucket}} = 12.5$ ns and always five or six bunches will arrive within an integration time at the detector. Consequently, a much lower fluctuation level of particles detected in subsequent detector integration times can be achieved. The generation of bunches with such a high rf frequency results in a significantly faster synchrotron motion because $Q_s \propto \sqrt{h}$.

VI. MACROSCOPIC SPILL STRUCTURES ARISING FROM FAST SYNCHROTRON MOTION

It is shown in Sec. IV that there is an optimum of the synchrotron tune above which the level of spill microstructures is again increased for further increased Q_s. An additional limitation to the improvement of the spill quality found in our studies is that synchrotron motion with sufficiently large synchrotron tune can result in the formation of macroscopic spill structures of a duration ~ 0.1 s or longer. Such structures could be found for conditions of present SIS18 operation in measurements as well as in simulations, see Figs. 4 and 5. These figures show spills of the extraction Ar^{18+} beams at beam energy $E = 500$ MeV/u bunched with an rf voltage of amplitude $V_{\mathrm{rf}} = 12$ kV and harmonic number $h = 5$. Crossing synchrobetatron resonances could be identified in tracking simulations as a likely mechanism, see e.g., [29–31]. These resonances are defined by the condition

$$kQ_x + lQ_y + mQ_s = n. \tag{20}$$

k, l, m, n are integer numbers, where actually $k = 3$, $l = 0$, and $n = 3 \cdot Q_{x,\mathrm{r}} = 13$. In simulations, the exact time behavior of Q_x is known. Hence, it can be detected when such a resonance is crossed. In doing so, a clear correlation between the instants when Q_x is fulfilling the resonance condition and the appearance of the structures could be found which one can see in Fig. 5. That figure makes it also visible that quadrupole ripples inhibit the formation of macroscopic structures, where the spill obtained with the quadrupole ripple of amplitude zero resembles more the measured spill in Fig. 4.

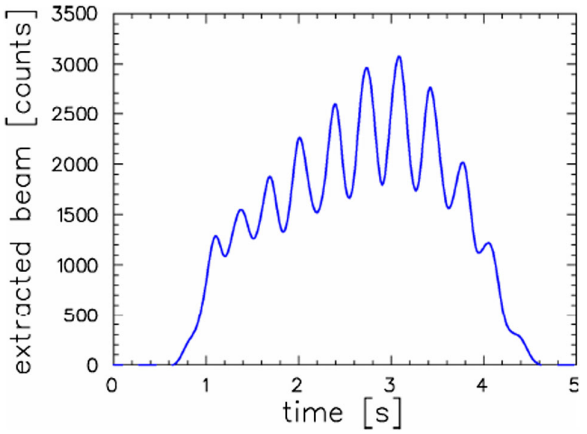

FIG. 4. Spill of an Ar^{18+} beam measured during slow extraction from SIS18 at the beam energy $E = 500$ MeV/u bunched with the rf voltage of amplitude $V_{rf} = 12$ kV and harmonic number $h = 5$.

The macroscopic structures are found to depend on the rf voltage, the horizontal beam emittance, and the momentum width. They become more visible for a higher rf voltage because the distance between subsequent intensity maxima or minima is larger such that the structures can be better resolved. In addition, the structures shown in Fig. 5 are found for bunches with a maximum momentum deviation $\delta_{max} = 5 \times 10^{-4}$ and a horizontal beam emittance

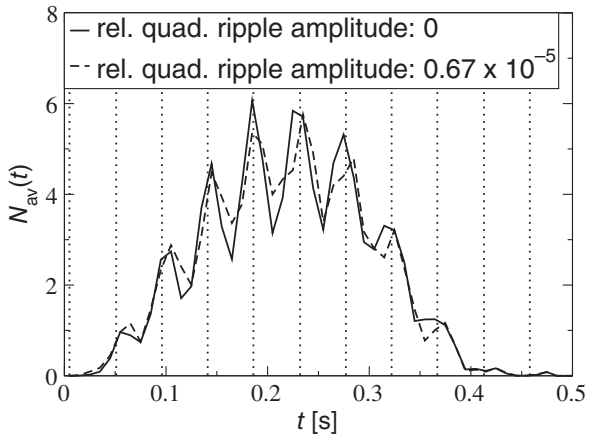

FIG. 5. Spill of an Ar^{18+} beam obtained in a slow extraction simulation for SIS18 conditions at the beam energy $E = 500$ MeV/u, where $V_{rf} = 12$ kV, $h = 5$, and quadrupole ripples of two different amplitudes are applied. The transverse beam emittances correspond to the machine acceptance at injection reduced by the factor of 0.2 and adiabatic shrinkage during acceleration afterward. Furthermore, the maximum momentum deviation in the bunches is $\delta_m = 5 \times 10^{-4}$. Both the transverse emittances and the maximum momentum deviation are lower than during the usual SIS18 operation. The dotted vertical lines mark the moments when the machine tune crosses a synchrobetatron resonance. The third integer resonance corresponding to $m = 0$ in Eq. (20) is crossed at $t = 0.41$ s.

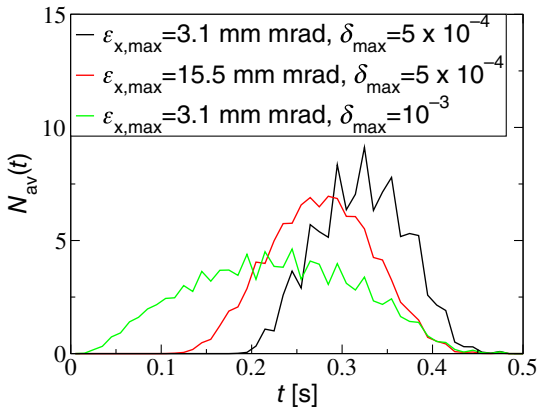

FIG. 6. Spills obtained for Ar^{18+} beam at beam energy $E = 500$ MeV/u bunched with the rf voltage of harmonic number $h = 5$ and amplitude $V_{rf} = 12$ kV with varied horizontal emittance and momentum width. The black curve corresponds to the solid black curve in Fig. 5, where the initial horizontal tune is changed from $Q_{x,ini} = 4.329$ in the figure above to $Q_{x,ini} = 4.327$ in this figure in order to enable the application of increased horizontal emittance and momentum width.

$\varepsilon_x = 3.1$ mm mrad. The latter is achieved by choosing a distribution of the initial transverse particle coordinates which corresponds to a total machine acceptance filled to 20% at injection and subsequent adiabatic shrinkage during acceleration. Both values are lower than during regular SIS18 operation. The structures are diminished or even vanish if the horizontal emittance or the momentum width is increased. It turns out that the horizontal emittance has a stronger influence than the momentum width which is demonstrated by repeating the simulations with increased momentum width and horizontal emittance, respectively. The resulting spills are shown in Fig. 6. They suggest that macroscopic spill structures should not play an important role in present SIS18 operation.

The situation will be different if the harmonic number of the rf field h is increased by a factor of about 20 which will result in a significantly increased synchrotron tune. That is demonstrated in the following by examining the example of an Ar^{18+} beam extracted at the same energy as in the example above but the harmonic number increased to $h = 100$. In the first step, the rf voltage amplitude $V_{rf} = 70$ kV is assumed which is planned to be the maximum of the high frequency cavity foreseen to be installed in SIS18 [18]. The resulting spill obtained by particle tracking is shown in the upper graph of Fig. 7.

The horizontal tune in this example is shifted from $Q_{x,i} = 4.326$ to $Q_{x,f} = 4.334$. The synchrotron tune is $Q_s = 0.015$ such that the gap between two synchrobetatron resonances is a little lower than 3 times the horizontal tune interval crossed during the extraction, $\Delta Q_x = 0.024$. Two resonances are crossed. They are marked by the dotted lines in the upper graph of Fig. 7, where the horizontal third integer resonance is that crossed at $t = 0.48$ s. In addition,

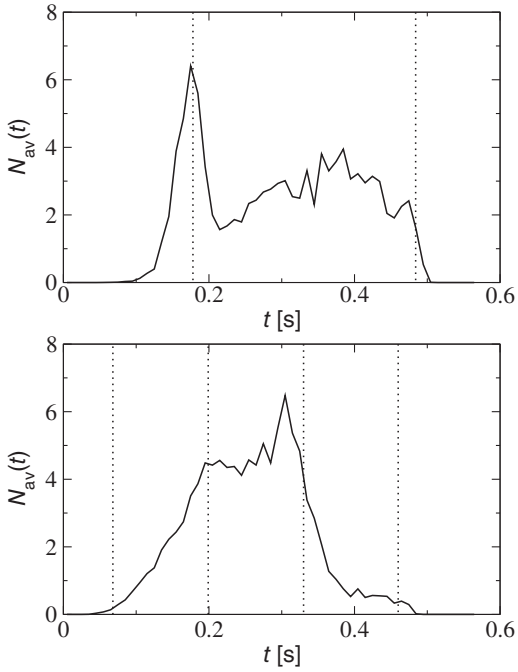

FIG. 7. Spills of the extraction of Ar^{18+} beams at beam energy $E = 500$ MeV/u bunched with rf fields of the harmonic number $h = 100$ obtained by particle tracking. Upper graph: The rf voltage $V_{rf} = 70$ kV is applied and the horizontal tune is moved from $Q_{x,i} = 4.326$ to $Q_{x,f} = 4.334$. Lower graph: The rf voltage $V_{rf} = 5$ kV is applied and the horizontal tune is moved from $Q_{x,i} = 4.329$ to $Q_{x,f} = 4.334$. The dotted lines mark the crossed synchrobetatron resonances.

this figure shows that the extraction rate has its maximum near the resonance crossed first at $t = 0.18$ s. The reason is that the number of particles in the beam when reaching the third integer resonance is already significantly reduced.

A significant reduction of the influence of the synchrobetatron resonance crossing occurs for reduced rf voltage which is demonstrated in the second step. The lower graph of Fig. 7 shows a spill obtained in a simulation, where the rf voltage is reduced to $V_{rf} = 5$ kV and the horizontal tune interval is changed to $(Q_{x,i}, Q_{x,f}) = (4.329, 4.334)$. All other quantities are preserved from the previous example. Now, the synchrotron tune is $Q_s = 0.0041$ and 3 times the horizontal tune interval is $3(Q_{x,f} - Q_{x,i}) = 0.015$. Consequently, four resonances are crossed. The figure shows that the maximum extraction rate occurs between crossing the second and the third crossed resonance. That is a sign that both these resonances are smeared out because they are closer to each other than for $V_{rf} = 70$ kV and because the synchrotron tune varies with the synchrotron amplitude.

However, the goal of the planned installation of the high harmonic rf cavity is the reduction of spill microstructures. Figure 8 shows the time dependent duty factors obtained in the simulations for $h = 100$ and both considered rf voltages, $V_{rf} = 5$ kV and $V_{rf} = 70$ kV, compared with that

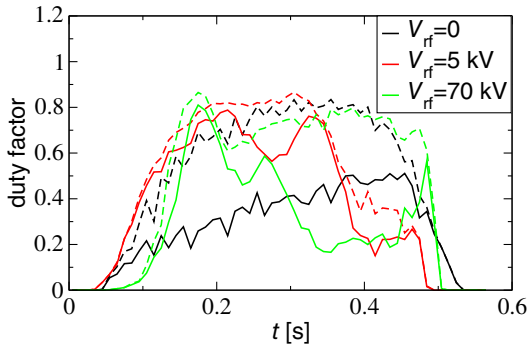

FIG. 8. Duty factors that correspond to the spills in Fig. 7 compared to that obtained with $V_{rf} = 0$, i.e., without bunching. The dashed curves represent the Poisson duty factors.

obtained for extraction of the unbunched beam. The duty factors found for both rf voltages are at the beginning of the extraction time interval higher than that obtained for the unbunched beam. The duty factor reduction toward the end of the spill found for $V_{rf} = 5$ kV is, basically, caused by the reduction of the extraction rate which is denoted by the simultaneous reduction of the Poisson duty factor and which can be seen in the lower graph of Fig. 7. In contrast to that, the Poisson duty factor as well as the corresponding spill shown in the upper graph of Fig. 7 are not reduced in the second half of the extraction. Hence, that duty factor reduction arises from an increase in the micro spill structure level. These results indicate that an improvement of the spill quality on microstructure level for the rf frequency increased by an order of magnitude is possible, where the spill microstructure mitigation is more efficient when applying a lower rf voltage.

VII. SUMMARY

We investigated the validity of spill microstructure improvement by bunched beam extraction for large synchrotron tunes. That was primarily motivated by the plan to install an rf cavity with an rf frequency of $f_{rf} = 80$ MHz in the GSI heavy ion synchrotron SIS18 which is approximately 20 times the rf frequency of the present cavity.

Our study revealed spill improvement by increasing the synchrotron tune only up to an optimum synchrotron tune and diminution of the spill quality when increasing the synchrotron tune beyond the optimum. The latter arises from the recapture of particles due to the synchrotron motion. That recapture keeps particles longer in the vicinity of the edge of the stable phase space area which is oscillating due to the tune ripples. Therefore, the spill quality defined by microstructures becomes worse at higher cavity voltages.

In addition, fast synchrotron motion is found in simulations and spill measurement to cause the formation of macroscopic spill structures of duration ~ 100 ms.

Crossing synchrobetatron resonances during the tune sweep is identified as the source. The structures are better visible for a higher synchrotron tune because the distance between the resonances is proportional to the synchrotron tune. Consequently, the structures are closer to each other and overlap for a lower synchrotron tune such that they are smeared out. For that reason, the rf voltage should be set as low as possible in order to inhibit the formation of macroscopic spill structures. Furthermore, it was shown that the formation of the macroscopic structures can be reduced by increasing the momentum width or the transverse emittance in the phase space plane used for the extraction, where the latter has a stronger impact.

Generally, the formation of macroscopic spill structures as well as the diminution of spill quality denote, in principle, limitations to the possibility to mitigate spill microstructures by increasing the synchrotron tune in order to reduce the duration of stay of particles near the separatrix.

[1] L. Badano, M. Benedikt, P. J. Bryant, M. Crescenti, P. Holy, A. Maier, M. Pullia, and S. Rossi, Proton-ion medical machine study (PIMMS) part I, Report No. CERN/PS/99-010 (DI), Geneva, 1999, https://cds.cern.ch/record/385378/files/ps-99-010.pdf.

[2] L. Badano, M. Benedikt, P. Bryant, M. Crescenti, P. Holy, P. Knaus, A. Maier, M. Pullia, and S. Rossi, Synchrotrons for hadron therapy: Part I, Nucl. Instrum. Methods Phys. Res., Sect. A **430**, 512 (1999).

[3] K. Hiramoto and M. Nishi, Resonant beam extraction scheme with constant separatrix, Nucl. Instrum. Methods Phys. Res., Sect. A **322**, 154 (1992).

[4] C. Krantz, T. Fischer, B. Kröck, U. Scheeler, A. Weber, M. Witt, and Th. Haberer, Slow extraction techniques at the Marburg ion-beam therapy centre, in *Proceedings of 9th International Particle Accelerator Conference, IPAC 2018, Vancouver, BC, Canada* (JACoW, Geneva, Switzerland, 2018), TUPAL036.

[5] D. Naito, Y. Kurimoto, R. Muto, T. Kimura, K. Okamura, T. Shimogawa, and M. Tomizawa, Real-time correction of betatron tune ripples on slowly extracted beam, Phys. Rev. Accel. Beams **22**, 072802 (2019).

[6] S. Sorge, P. Forck, and R. Singh, Measurements and simulations of the spill quality of slowly extracted beams from the SIS-18 synchrotron, J. Phys. Conf. Ser. **1067**, 052003 (2018).

[7] R. Singh, P. Forck, and S. Sorge, Reducing Fluctuations in Slow-Extraction Beam Spill Using Transit-Time-Dependent Tune Modulation, Phys. Rev. Appl. **13**, 044076 (2020).

[8] T. Furukuwa and K. Noda, Contribution of synchrotron oscillation to spill ripple in RF-knockout slow-extraction, Nucl. Instrum. Methods Phys. Res., Sect. A **539**, 44 (2005).

[9] P. Forck, H. Eickhoff, A. Peters, and A. Doliniskii, Measurements and improvements of the time structure of slowly extracted beam from a synchrotron, in *Proceedings of the European Particle Accelerator Conference, Vienna, 2000* (EPS, Geneva, 2000), p. 2237, MOP4B03.

[10] R. Cappi and Ch. Steinbach, Low frequency duty factor improvement for the CERN PS slow extraction using RF phase displacement techniques, IEEE Trans. Nucl. Sci. **28**, 2806 (1981).

[11] S. v. d. Meer, Stochastic extraction, a low-ripple version of resonant extraction, Report No. CERN-PS-AA-78-6, 1978.

[12] K. A. Brown, L. Ahrens, J. M. Brennan, J. W. Glenn, M. Sivertz, and S. R. Koscielniak, Mini-bunched and micro-bunched slow extracted beams from the AGS, in *Proceedings of the 9th European Particle Accelerator Conference, Lucerne, Switzerland, 2004* (JACoW, Geneva, 2004), p. 1544.

[13] J. W. Glenn, L. Ahrens, T. Hayes, and R. Lee, Mini-bunching the AGS slow external beam, in *Proceedings of the Particle Accelerator Conference, Vancouver, BC, Canada, 1997* (IEEE, New York, 1997), p. 965.

[14] L. Ahrens *et al.*, Interbunch extinction measurement at the BNL AGS for the KOPIO experiment, Nucl. Instrum. Methods Phys. Res., Sect. A **560**, 256 (2006).

[15] V. Nagaslaev, J. Amundson, J. Johnstone, L. Michelotti, C. S. Park, S. Werkema, and M. Syphers, Third integer resonance slow extraction scheme for a $\mu \rightarrow e$ experiment at Fermilab, in *Proceedings of the 46th ICFA Advanced Beam Dynamics Workshop on High-Intensity and High-Brightness Hadron Beams, HB2010, Morschach, Switzerland* (2010), p. 153, MOPD40, https://accelconf.web.cern.ch/HB2010/papers/mopd40.pdf.

[16] Y. Fukao *et al.*, Measurement of proton beam profile at 8 GeV acceleration commissioning for the J-PARC COMET experiment, in *Proceedings of PASJ2018, Nagaoka, Japan* (2018), p. 231, FROL12, https://www-linac.kek.jp/mirror/www.pasj.jp/web_publish/pasj2018/proceedings/PDF/FROL/FROL12.pdf.

[17] SHiP Collaboration, The SHiP experiment at the proposed CERN SPS Beam Dump Facility, Eur. Phys. J. C **82**, 486 (2022).

[18] P. Schmid, Planned measures for improving the SIS18 spill quality, in *Proceedings of Slow Extraction Workshop, CERN, Geneva, Switzerland, 2017*, see https://indico.cern.ch/event/639766.

[19] HADES Collaboration, The high-acceptance dielectron spectrometer HADES, Eur. Phys. J. A **41**, 243 (2009).

[20] J. Pietraszko, Slow extraction—input from HADES at SIS18, in *Proceedings of HIC4FAIR Workshop, Darmstadt, Germany, 2016*, see https://indico.gsi.de/event/4570.

[21] J. Pietraszko, The HADES/CBM physics case requirements, in *Proceedings of Slow Extraction Workshop, Darmstadt, Germany, 2016*, see https://indico.gsi.de/event/4496.

[22] Y. Kobayashi and H. Takahashi, Improvement of the emittance in the resonant beam ejection, Proceedings of 6th International Conference on High-Energy Accelerators, Cambridge, MA, USA, edited by R. A. Mack (Cambridge by Cambridge Electron Accelerator, 1967), p. 347, https://inspirehep.net/files/92350bdcf9bf65f0baafd25d18a60d36.

[23] W. Hardt, Ultraslow extraction of LEAR, CERN, Report No. PS/DL/LEAR Note 81-6, $\bar{p}p$ LEAR Note 98, 1981.

[24] M. Pullia, Detailed dynamics of slow extraction and its influence on transfer line design, Ph.D. thesis, Université Claude Bernard-Lyon, 1999.

[25] R. Singh, P. Forck, P. Boutachkov, S. Sorge, and H. Welker, Slow extraction spill characterization from micro to millisecond scale, J. Phys. Conf. Ser. **1067**, 072002 (2018).

[26] S. Y. Lee, *Accelerator Physics, Second Edition* (World Scientific Publishing Co. Pte. Ltd, Singapore).

[27] B. Franczak, SIS Parameter List, GSI, Darmstadt, Report No. GSI-SIS-TN/87-13, 1987.

[28] T. Milosic, R. Singh, and P. Forck, Sub-ns single-particle spill characterization for slow extraction, in *Proceedings of 10th International Beam Instrumentation Conference, Pohang, Republic of Korea, 2021* (2021), p. 438, WEPP28, https://accelconf.web.cern.ch/ibic2021/papers/wepp28.pdf.

[29] T. Suzuki, Synchro-betatron resonances, Part. Accel. **27**, 157 (1990), https://cds.cern.ch/record/201687/files/p157.pdf.

[30] S. Y. Lee, Single particle dynamics at synchro-betatron coupling resonances, Phys. Rev. E **49**, 5706 (1994).

[31] A. Piwinski, Synchro-betatron resonances, in *Proceedings of CAS - CERN Accelerator School: Accelerator Physics, Oxford, UK* (1985), p. 187, https://cds.cern.ch/record/173739/files/p187.pdf.